JOURNAL OF GEOPHYSICAL RESEARCH, VOL. 103, NO. D3, PAGES 3599–3610, FEBRUARY 20, 1998

Low-ozone pockets explained

Gary A. Morris,[1] S. R. Kawa, A. R. Douglass, and M. R. Schoeberl
NASA Goddard Space Flight Center, Greenbelt, Maryland

L. Froidevaux and J. Waters
Jet Propulsion Laboratory, California Institute of Technology, Pasadena

Abstract. Pockets of low ozone have been observed on numerous occasions in anticyclones at middle to high latitudes in the middle stratosphere. Air masses within the anticyclones at altitudes near 850 K ($\sim$ 32 km) contain $\sim$ 25% less ozone than the surrounding air. Trajectory calculations have revealed that much of the air within the pockets originates in the tropics or subtropics at higher altitudes several weeks earlier. Previous studies have, however, left unanswered a number of questions related to the formation of the low-ozone regions. Using a Lagrangian chemical model with initialization based upon observations from the Upper Atmosphere Research Satellite (UARS), we examine in detail an event in March 1993. Our results demonstrate that the development of the observed ozone pockets can be explained with our current understanding of chemistry and dynamics. The primary mechanism responsible for the development of these low-ozone regions is the isolation of air at high latitudes for periods of time long enough that significant ozone loss toward the local photochemical equilibrium can occur. Such behavior is different from that of the surrounding air masses that move from middle to high latitudes and back again over the course of a few days. The dynamical behavior associated with these latter air masses results in ozone concentrations more consistent with lower-latitude equilibrium values.

1. Introduction

In the middle stratosphere, the lowest ozone mixing ratios are typically found within the winter polar vortex, owing to both chemistry and dynamics. The limb infrared monitor of the stratosphere (LIMS) [*Leovy et al.*, 1985] and the Microwave Limb Sounder (MLS) [*Manney et al.*, 1995], however, have frequently detected air masses in the winter hemisphere, outside the vortex, with similarly low ozone mixing ratios. These low-ozone pockets typically extend from 20 to 2 mbar (27–43 km or 750–1250 K). *Leovy et al* [1985] note that the regions of low ozone seen in the LIMS data develop in middle to late winter in conjunction with stratospheric wave breaking events. During these events, air masses with relatively high amounts of ozone move northward over the polar cap, while a pool of low ozone forms in a strong anticyclone.

Plate 1 shows one of these events, described by *Manney et al.* [1995], as observed by MLS on the 850 K potential temperature surface ($\sim$ 32 km) at 0000 GMT, March 9, 1993. Three days of MLS ozone (version 3) measurements were used to construct this synoptic, Barnes–gridded trajectory map [*Morris et al.*, 1995] (more details can be found in section 3.2). The bold white line indicates the edge of the polar vortex as defined by the 5×10^{-4} (K m^2)(kg s)$^{-1}$ National Centers for Environmental Prediction (NCEP) potential vorticity (PV) contour. As *Manney et al.* [1995] note, the polar vortex is shifted off the pole during a stratospheric warming event, and a strong anticyclone (the Aleutian high) has set up over North America. Each of these dynamical features coincides with a region of low ozone. Relatively high values of ozone (more typical of midlatitudes) extend over the polar cap, separating the two regions of low ozone. The formation of the low-ozone region centered over Europe, inside the polar vortex, is familiar. The one in the anticyclone over Canada, however, evolves quite differently and is the subject of this paper.

[1]Now at Joint Center for Earth Systems Technology, University of Maryland Baltimore County, Baltimore.

Paper number 97JD02513.
0148-0227/98/97JD-02513$09.00

2. Air Mass Origins

To determine the origin of this air, it is helpful to examine the water vapor field. Water vapor has a longer lifetime than ozone at this altitude, so it serves as an accurate tracer of stratospheric motion [*Brasseur and*

Solomon, 1984]. Plate 2 shows a map of the MLS water vapor field (version 3) on March 9, 1993, at 850 K (32 km). As expected, low water mixing ratios (4–5 ppmv) are seen in the tropics, while higher values (6–7 ppmv) appear inside the vortex. In this map, we also observe a region over Canada with low water vapor values similar to the tropical observations. The location of this low water vapor region is well correlated with the location of the low ozone pocket seen in Plate 1. If the air within the low-ozone pocket had its origins within the vortex, we would have expected the associated water vapor field to be high. The low-ozone pocket therefore does not come from the vortex.

As *Manney et al.* [1995] show, vertical motion is not solely responsible for the pocket either. Vertical profiles of water vapor show increasing values with altitude due to CH_4 photolysis in the upper stratosphere and mesosphere [*LeTexier et al.*, 1988]. Although strong descent could lead to decreases in the observed ozone mixing ratio at polar latitudes in the middle stratosphere, it would also lead to increases in the water vapor mixing ratio, contradicting the observations. The water vapor data therefore most strongly suggest tropical origins for the air contained within the pockets.

Manney et al. [1995] extensively examined the dynamics associated with the formation of low-ozone pockets. In each case, a pocket develops several days after the peak of a stratospheric warming. Trajectory calculations indicate that air within the pockets originates in the tropics or subtropics 2–3 weeks earlier, is transported northward through a warm region, and develops an anticyclonic rotation (as would be expected for parcels moving isentropically away from the equator in accordance with the conservation of potential vorticity [*Holton*, 1992]). Radiative transfer calculations, based on the middle atmosphere radiation code (MIDRAD) [*Manney et al.*, 1995; *Shine*, 1987], indicate the air mass descends 3–7 K/d ($\sim 0.1-0.2$ km/d) on average during the course of the event.

Along 21–day air parcel trajectories, ozone decreases by as much as 50% from initially high values ($\sim$ 10 ppmv) in the tropics to much lower values (5–6 ppmv) in the pocket. An increase in HNO_3 [*Manney et al.*, 1995; *Rood et al.*, 1993] is also observed in association with the development of the low-ozone pockets.

Manney et al. [1995] lists a number of issues related to the formation of low-ozone pockets that need to be explained by modeling efforts, among them are the following: the pockets appear in the anticyclone several days after the peak of a stratospheric warming; they are confined vertically to the region between 15 and 5 hPa; they appear downstream of a warm region; they originate in the tropics; they contain air parcels which have been confined together for 1–3 weeks; and they contain enhanced amounts of HNO_3.

We have examined several events of this type using a Lagrangian chemical model [*Kawa et al.*, 1993] in an attempt to address these issues. All of our studies lead to similar conclusions. In this paper, we present a detailed analysis for the case of February–March 1993. In the next section, we describe the trajectory calculations and the UARS–based initialization of the chemical model. We then provide results from our February–March 1993 study and compare model output to the satellite observations. Next, we demonstrate that the ozone pockets result from dynamical isolation of air masses at middle to high latitudes for periods long enough that the local photochemical equilibrium can be approached. This behavior contrasts that of the surrounding air masses, which spend relatively short periods of time at high latitudes and which retain ozone concentrations more consistent with the midlatitude photochemical equilibrium. We then address the issues of nitric acid enhancement and the sensitivity of our results to changes in a variety of model inputs. Finally, we demonstrate the consistency of our model with UARS observations for 2 other events: December 1992 in the northern hemisphere and September 1992 in the southern hemisphere.

3. Modeling

We examine the February–March 1993 event using a Lagrangian chemical model that requires two types of inputs: air parcel trajectory information (including position and temperature data) and a chemical initialization (including overhead ozone amounts along the calculated trajectories). Trajectory model calculations provide the former, while UARS data yield the latter. The chemical model contains more than 100 reactions on more than 30 species, includes updated photolysis tables (based upon *Anderson et al.* [1995]) and heterogeneous chemistry, and conserves NO_y, Cl_y, and H_2O (for more model details, see *Kawa et al.* [1993]). Photolysis cross sections are taken from *DeMore et al.* [1994]. The calculated photolysis rates compare well with the benchmark developed for the Atmospheric Effects of Aircraft Program [*Stolarski et al.*, 1995].

3.1. Dynamics

We employ the Goddard trajectory model [*Schoeberl and Sparling*, 1995] and heating rates calculated according to *Rosenfield* [1991] to determine 22–day, diabatic back trajectories for 934 parcels in the northern hemisphere. These parcels are initialized at 0000 GMT March 9, 1993, on a near–uniform spatial density grid at 850 K ($\sim$ 32 km) such that the number of parcels N_i at a given latitude λ_i is given by

$$N_i \simeq N_0 \cos\lambda_i \qquad (1)$$

where N_0 is the number of parcels at the equator and $\lambda_i = 5i$ for $0 \leq i \leq 18$. Balanced winds from NCEP drove the parcel trajectories [*Randel*, 1987; *Newman, et al.*, 1988]. Our diabatic trajectory calculations show good agreement with the calculations of *Manney et al.* [1995]. While no individual trajectory can be accurate for calculations of such duration, the ensemble behavior of a large number of such trajectories is reliable, as shown by *Morris et al.* [1995].

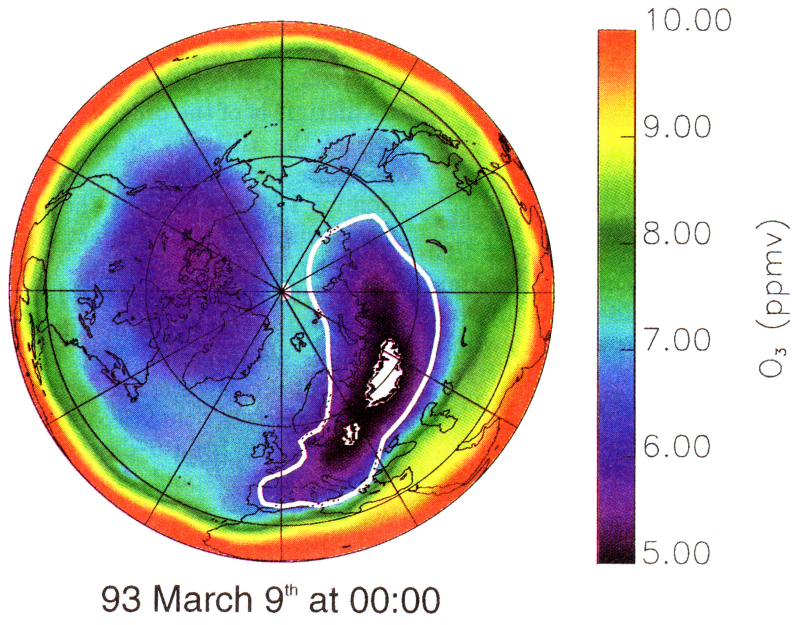

Plate 1. Barnes trajectory map of Microwave Limb Sounder (MLS) ozone data at 0000 GMT on March 9, 1993, on the 850 K (~32 km) surface. The MLS data that were gathered within +/- 1.5 days of this time have been synoptically mapped using the trajectory mapping technique and then gridded using a Barnes scheme [*Morris et al.*, 1995]. The bold white line represents the boundary of the vortex as defined by the 5×10^4 K $m^2/kg/s$ National Centers for Environmental Prediction potential vorticity contour. Notice the region of low ozone outside the vortex over Canada. White regions indicate data values below 5 ppmv.

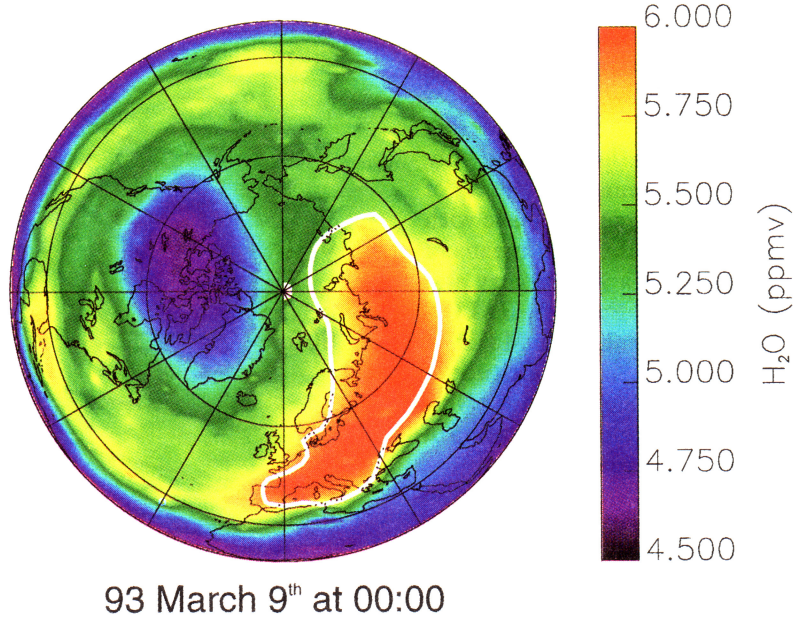

Plate 2. Trajectory map of MLS water vapor data mapped as in Plate 1. The region of low water vapor outside the vortex over Canada coincides with the region of low ozone outside the vortex seen in Figure 1.

3.2. Chemistry

The chemical initialization uses nighttime measurements of HNO_3 and $ClONO_2$ (version 7) from the Cryogenic Limb Array Etalon Spectrometer (CLAES) and sunset measurements of NO and NO_2 (version 17) from the Halogen Occultation Experiment (HALOE) to estimate total odd nitrogen (NO_y). Total inorganic chlorine (Cl_y) consists of HALOE measurements of HCl (version 17) and CLAES measurements of nighttime $ClONO_2$. At the altitudes relevant to our study, our estimates of NO_y and Cl_y should be accurate to within 5–10% [*Morris et al.*, 1997; *Dessler et al.*, 1995]. Further, the model is insensitive to changes in NO_y and Cl_y of this magnitude, as discussed in section 5.3. Version 3 MLS measurements of H_2O and O_3 (both mixing ratio and upper stratospheric column measurements) and version 7 CLAES measurements of CH_4 are also used in the initialization of the model. Validations of these UARS data have been published in the "Evaluation of the UARS Data" special issue of the *Journal of Geophysical Research, 101*(D6), 9539–10,476, 1996.

With the exception of the ozone mixing ratios, zonal mean calculations provide the initial values for the input chemical constituents. We determine zonal means every 5° of latitude on potential temperature surfaces spaced every 100 K between 700 and 1100 K (28–37 km). We then interpolate these data horizontally to the latitude positions and vertically to the pressure levels of each of our model air parcels on February 15, 1993, as determined from the diabatic back trajectory calculations.

Around the time of the model initialization (February 12–15), the vortex appears displaced off the pole toward Europe by a large wave 1 event. Despite the asymmetry in the dynamic state, the inaccuracies caused by a zonal mean initialization have little effect on the final values of ozone predicted by the Lagrangian chemical model (see section 5.3). Zonal means of the CLAES and MLS data consist of 1–week averages centered on February 15, 1993. HALOE zonal means, however, consist of averages over much longer periods. Because HALOE is a solar occultation instrument and gathers data in only two latitude bands each day, approximately 1 month of HALOE data is required to construct zonal means with global coverage. We therefore compute zonal means of the sunset HALOE NO and NO_2 data in February and April of 1993 and average the results. For HCl, HALOE sunrise and sunset data from January through March of 1993 are binned and zonally averaged. At the altitude of our study, the zonal mean HCl field changes slowly with time, permitting a sufficiently accurate determination of HCl for our initialization with this procedure.

To capture the meridional structure in the initial MLS ozone field, we employ the trajectory mapping technique [*Morris et al.*, 1995]. In brief, trajectory mapping creates synoptic maps of constituent fields by isentropically advecting measurements forward or backward from the time and location at which they are made to a specified time. The mixing ratio of the transported species is assumed to be conserved along the calculated trajectory.

The MLS ozone trajectory map consists of measurements made within ±1.5 days of 0000 GMT February 15, 1993. Although ozone is not a conserved trace gas, its lifetime is of the order of a week (except in the tropics) at the altitudes of our study (see Figure 1). We therefore expect that the assumption of passive advection for 1.5 days used by the trajectory mapping technique will have little impact on the uncertainty of the resulting MLS ozone maps.

As further evidence of the validity of this assumption, we use estimates of the maximum rates of ozone change over our study period from *Manney et al.* [1995]. In the most severe case, ozone changes by ~ 2% per day along trajectories that become confined in the low-ozone pockets. Over the 1.5–day trajectory calculations, such ozone changes would result in ~ 3% uncertainties in the trajectory–mapped ozone measurements. Such uncertainties are less than those associated with the MLS measurements themselves, which are estimated to carry 3% precision and 5% accuracy uncertainties [*Froidevaux et al.*, 1996] (see also Table 1). For comparison with the results obtained using a trajectory mapped ozone initialization, we also ran a case with a zonal mean ozone initialization and found no significant differences in our results (see also section 5.3). Finally, overhead column ozone along each trajectory is parameterized as a function of latitude in the model from a zonal mean MLS climatology generated over the 22–day study period.

4. Results

4.1. Chemical Model Simulation

After the trajectory positions and chemical initialization from February 15 are input, the chemical model is

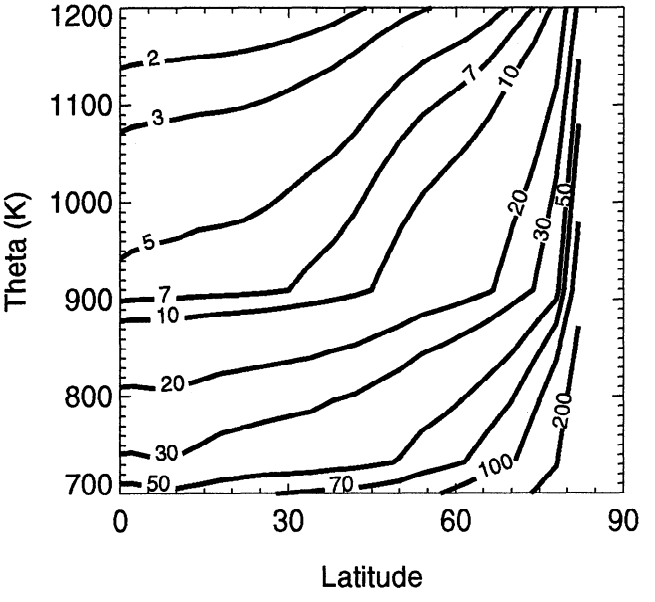

Figure 1. Ozone photochemical lifetime (days) based on ozone loss rates as calculated by the Goddard three-dimensional chemistry and transport model for March 1.

Table 1. Accuracy Uncertainty Estimates for UARS

Instrument	Constituent	Accuracy, %	Location
CLAES	HNO_3[a]	6–15	below 8 ppbv
	CH_4[b]	15	46–0.46 mbar
	$ClONO_2$[c]	35	above 10 mbar
		28	at 10 mbar
HALOE	NO[d]	15	above 21 mbar
	NO_2[d]	15	above 21 mbar
	HCl[e]	~15	
MLS	O_3[f]	5	22–2 mbar
	H_2O[g]	9	10 mbar

Abbreviations are CLAES, cryogenic limb array etalon spectrometer; HALOE, Halogen Occultation Experiment; and MLS, Microwave Limb Sounder.

[a] *Kumer et al.* [1996].
[b] *Roche et al.* [1996].
[c] *Mergenthaler et al.* [1996].
[d] *Gordley et al.* [1996].
[e] *Russell et al.* [1996].
[f] *Froidevaux et al.* [1996].
[g] *Lahoz et al.* [1996].

run forward in time through March 9, 1993. Plate 3 shows the resulting model ozone field at 0000 GMT on March 9. The comparison with MLS ozone data (Plate 1) is quite good: Both model and MLS see low ozone (~ 5 ppmv) within the vortex boundary (the bold white line in the plate); both also show high values in the tropics (> 10 ppmv); and both depict low ozone (< 6 ppmv) in the region of the anticyclone over northern Canada.

Figure 2 shows a scatterplot of the model and MLS measured ozone values at the ~ 3500 grid points to which the data sets have been interpolated with a Barnes scheme. The agreement is very good, particularly for lower values of ozone. We find ~ 5.5% root mean square differences between the model calculations and MLS measurements for ozone values less than 8 ppmv. Again, this compares well with the estimated uncertainty of the MLS data (see Table 1). For ozone values greater than 8 ppmv, the MLS data are systematically higher than model predictions by 8–11%.

Figure 3 shows the zonal mean MLS and model ozone data in 5° latitude bins. The figure demonstrates good agreement between the MLS and model ozone data for latitudes north of 20°N. The low-ozone pocket itself actually has little impact on the zonal mean ozone at this altitude and time (calculations including and excluding the low-ozone pocket result in ~ 2% changes in the zonal mean). In the tropics, MLS appears higher than the model by ~ 10%. Other studies also indicate that tropical ozone values from MLS in the midstratosphere are larger than ozonesonde and Stratospheric Aerosol and Gas Experiment II (SAGE II) data by about 5% [*Cunnold et al.*, 1996; *Froidevaux et al.*, 1996]. Model ozone values in the tropics show good agreement with measurements from both HALOE and the solar backscatter ultraviolet 2 (SBUV2) instrument, as well as with model calculations of the photochemical equilibrium.

Figure 3 also shows the photochemical equilibrium values of ozone at latitudes between the equator and 70°N for March 9, 1993. To determine the photochemical equilibrium ozone in a manner consistent with our ozone pocket study, we initialize a single parcel every 5° of latitude between 0° and 70°N on February 15, 1993, using the UARS zonal mean data. These parcels remain fixed in space while being run forward in time for 22 days to March 9, 1993. The solar zenith angles and temperatures are constrained to repeat the conditions of March 9, 1993; on two hundred successive model days. The final state of the model thereby represents photochemical equilibrium for March 9.

Figure 3 indicates that the local ozone values measured by MLS and predicted by the model match the photochemical equilibrium values for latitudes between 15° and 45°N. North of 45°N, however, the observed ozone exceeds the photochemical equilibrium values. To maintain such a disparity, an influx of air high in ozone must be maintained. (A number of authors have discussed the importance of eddy transport from the tropics in this process, including *Tuck* [1979]; *Pyle and Rodgers* [1980]; and *Douglass et al.* [1997]). The low-ozone pockets therefore appear to represent regions in which this influx has been substantially reduced. As a result of isolation, ozone within the anticyclone can fall toward the local photochemical equilibrium value of 3.5–4.7 ppmv and attain values ≤ 5.5 ppmv by March 9.

4.2. Equivalent Solar Latitude

The extent to which air within the anticyclone has been isolated at high latitudes can be seen in Plate 4. For each parcel included in our chemical calculations,

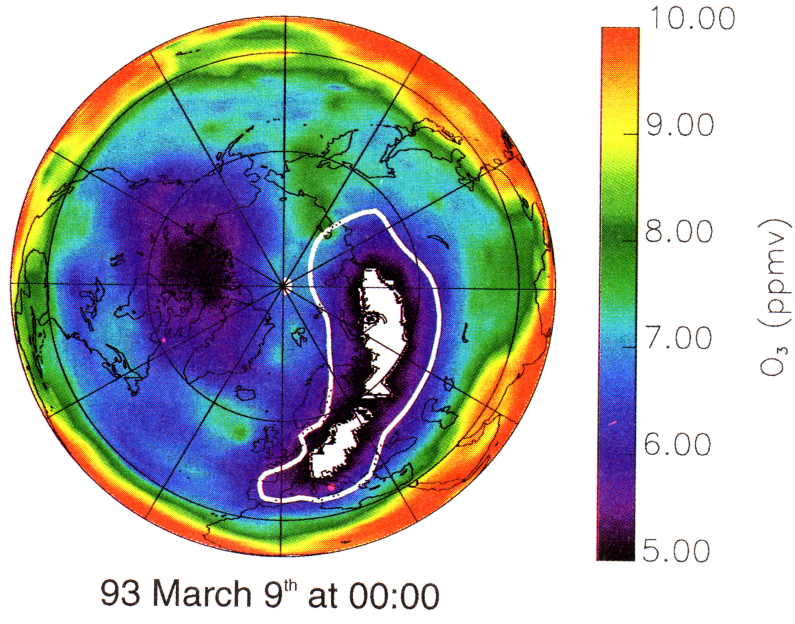

Plate 3. Barnes map of gridded output ozone from the Lagrangian chemical model [*Kawa et al.*, 1993] at 0000 GMT on March 9, 1993, on the 850 K surface. The Lagrangian model reproduces the observed ozone gradients, including low ozone in both the vortex and the anticyclone. White regions indicate data values below 5 ppmv.

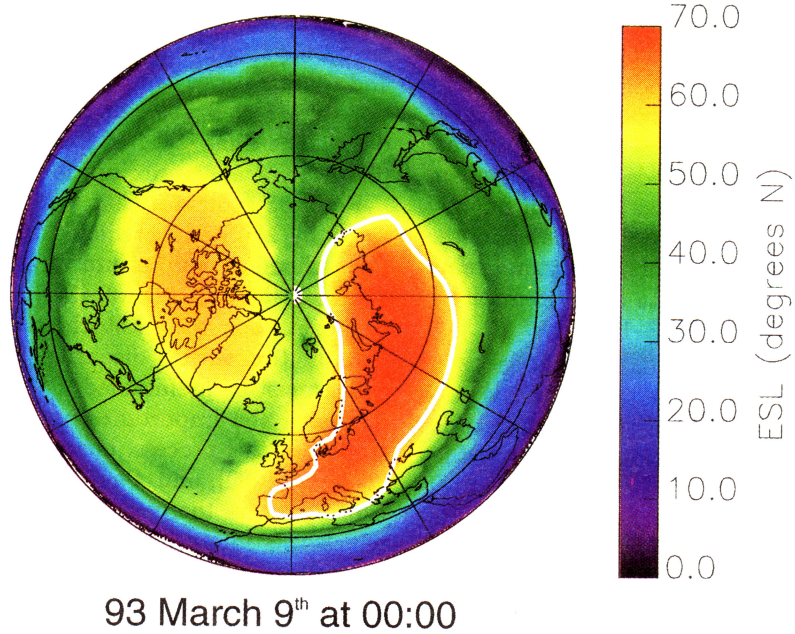

Plate 4. Equivalent solar latitude (see text) along 14-day, diabatic back trajectories for air parcels used in the trajectory chemical model on March 9, 1993, on the 850 K surface. Parcels surrounding the anticyclone have been exposed to significantly more sunlight than those trapped inside it. The solar exposure associated with parcels outside the anticyclone is typically found at 40°–50°N, while the solar exposure inside the anticyclone is typically found near 70°N.

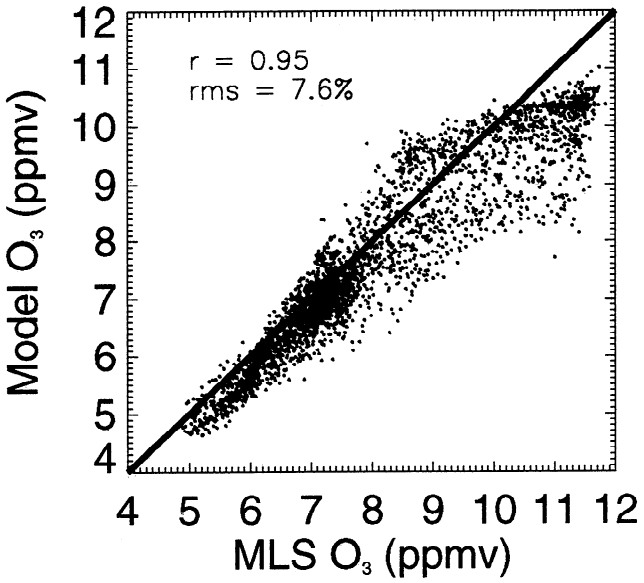

Figure 2. Model versus MLS ozone on the 850K surface at 0000 GMT on March 9, 1993.

we calculate the equivalent solar latitude (ESL), a quantity related to the dynamic history of an air parcel. To determine ESL, we first calculate the exposure to direct overhead sunlight (solar exposure) for each air parcel over the previous 14 days. The solar exposure is given by the integral of the positive values of the cosine of the solar zenith angle along the 14–day back trajectory. We then index the resulting quantity to the solar exposures calculated for parcels remaining at a constant latitude over the same 14–day period. This indexed quantity (ESL) (plotted in Plate 4) characterizes the latitude at which an air parcel with a given solar exposure would be found if it had remained at a fixed location in the atmosphere. For our dynamical analysis, ESL relates the solar weighted, average latitude at which an air parcel has been found over the previous 2–week period: Parcels with high ESL have spent most of their time at high latitudes, while parcels with low ESL have spent most of their time at low latitudes. Because the production and loss of ozone are dependent upon the total amount of sunlight and the solar zenith angle, ESL is highly correlated with ozone ($|r| > 0.95$) and more closely characterizes gradients in the ozone field than geographic latitude.

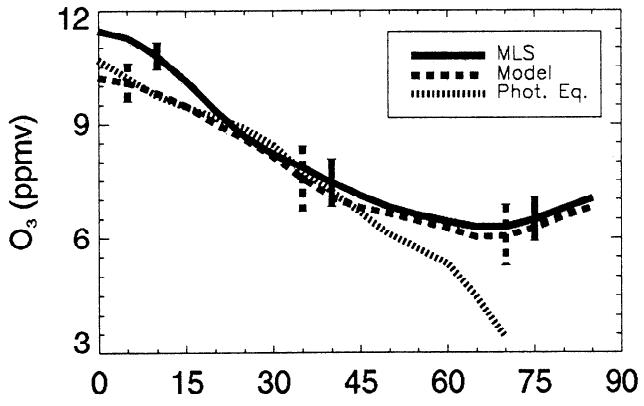

Figure 3. Zonal mean model, MLS, and photochemical equilibrium ozone as a function of latitude as determined from a chemical box model on the 850 K surface at 0000 GMT on March 9, 1993. Each zonal mean model and MLS bin represents an average over 5° latitude. Error bars represent 1σ variation in each bin for both the model and MLS. Photochemical equilibrium values were computed every 5° latitude from the equator to 70°N.

Examining the ESL field provides more insight into the relevant dynamical histories of the air parcels included in our chemical model simulations than examining individual trajectory calculations. As pointed out by *Morris et al.* [1995], individual trajectory calculations become inaccurate on relatively short timescales. However, the average behavior of large ensembles of trajectories is reliable over very long timescales (up to a month). Because the ESL field embodies the average behavior of a large number of trajectories, it provides more reliable information on the relative differences in the air parcel histories.

We first note that the ESL field of Plate 4 is very coherent and highly correlated with the MLS ozone field of Plate 1. A well-defined, isolated region of high ESL (low ozone) appears in the vicinity of the Aleutian anticyclone as well as within the polar vortex. Low ESL (high ozone) values are confined to the tropics, while intermediate values are found at midlatitudes and extend across the polar cap, separating the vortex and the anticyclone. High ESL values within the vortex and the anticyclone confirm that air parcels within these regions have been isolated at high latitudes for the previous two weeks. Many air parcels at the same or even higher geographic latitudes but outside these regions exhibit much lower ESL values, identifying air that has spent most of its time at lower geographic latitudes during the previous 2 weeks. An examination of individual air parcel trajectories (not shown) confirms these results. The isolation of air within the vortex and anticyclone at high latitudes (indicated by high ESL) differentiates these air masses from the surrounding air masses (with lower ESL) and is the most important factor responsible for their comparatively low ozone.

4.3. Conceptual Model

To demonstrate that the isolation of air parcels within the anticyclone is ultimately responsible for their relatively low ozone, we employ a conceptual model study summarized by Figure 4. We first construct two artificial, isentropic trajectories on the 850 K surface (shown as the solid lines in Figure 4b): One parcel (light gray and labeled "tangential") began at 40°N, moved north after 7 days, asymptotically approaching 70°N; the other parcel (black and labeled "oscillating") also began at 40°N and then oscillated between 40°N and 85°N with a period of ~ 4.8 days. The behavior of the former simulates that of air parcels that become trapped in the anticyclone. The behavior of the latter

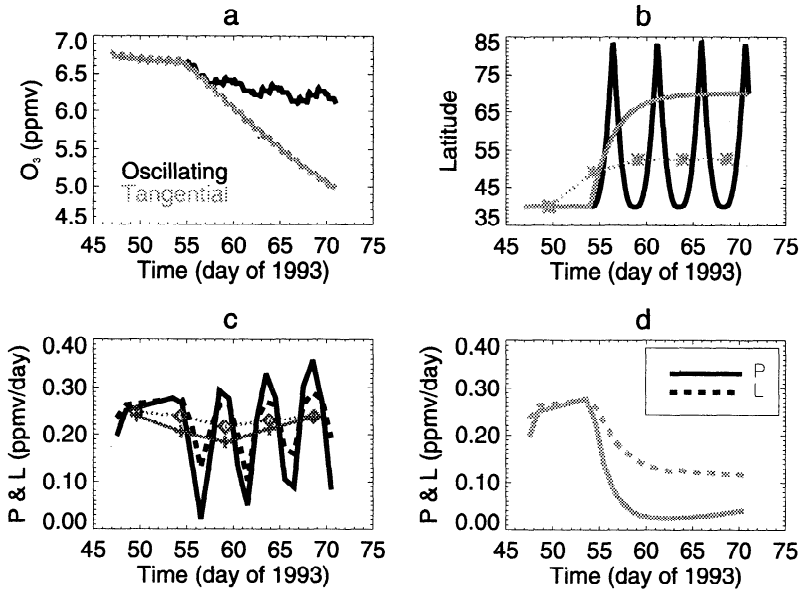

Figure 4. Conceptual model run of the Lagrangian chemical model over the same period of time as the actual low-ozone event (February–March 1993). Two artificial trajectories are input: one which oscillates between 40°N and 85°N and one which asymptotically approaches 70°N (trajectories shown in Figure 4b). The dotted line in Figure 4b represents a running 4.8–day average of the position of the oscillating parcel. The oscillating parcel contains more than 20% more ozone than the "tangential" parcel by the end of a 24-day run (shown in Figure 4a), despite identical initializations. Figures 4c and 4d show the production and loss of ozone for the oscillating and tangential cases, respectively. For the oscillating case (Figure 4c), the bold black lines represent diurnal averages, while the thin, dark gray lines represent running 4.8–day averages of the production and loss. Losses are indicated by the dashed lines, while productions are indicated by the solid lines.

simulates that of air parcels that circle the anticyclone and/or the vortex without becoming entrained in either. The artificial trajectories are representative of the air parcel motion indicated by back trajectory calculations with analyzed wind fields. (We have run these simulations with a variety of initial latitudes and note that the initial latitude selected has little impact on the results of this study.) By employing the artificially constructed trajectories, we eliminate the uncertainty in our results associated with the trajectory calculations, thereby allowing us to focus entirely on the effects on the chemical model calculations of differences in the dynamical histories of the air parcels. A zonal mean constituent initialization and a zonal mean temperature field were constructed for use in these Lagrangian chemical model calculations.

Figure 4 demonstrates how two parcels, which started at exactly the same geographic location with exactly the same chemical initialization, can end up in exactly the same geographic location with quite dissimilar values of ozone. Figure 4a depicts the ozone associated with each trajectory as a function of time. Notice that the oscillating parcel contains ~ 20% more ozone than the tangential parcel by the end of the 24–day simulation and that the ozone associated with the tangential parcel is still declining rapidly toward the local photochemical equilibrium (~ 3.5 ppmv for this latitude as shown in Figure 3).

The mechanism responsible for this difference is revealed by Figures 4c and 4d. The thick lines in these two figures show the diurnally integrated production and loss of ozone associated with each trajectory as a function of time. As the tangential parcel moves north, production falls off much more sharply than loss (shown in Figure 4d). Such behavior can be attributed to the fact that the photolysis of oxygen molecules, key to ozone production, drops off much more rapidly with latitude than the production of molecules that contribute to ozone loss (e.g., NO and ClO). As a result, loss exceeds production throughout the study period and significant ozone loss occurs.

In contrast, meridional motion repeatedly returns the oscillating parcel to low-latitude regions (seen in Figure 4b), resulting in more ozone production (Figure 4c) and slower ozone decay (Figure 4a). Production and loss alternately dominate the ozone chemistry, resulting in the oscillating behavior of ozone seen in Figure 4a. The overlying ozone trend associated with this parcel may best be understood through a comparison of its behavior with that of an equivalent tangential parcel.

To determine such a parcel, we plot a running average of the latitude of the oscillating parcel over the period

of oscillation (~ 4.8 days), shown by the dotted gray line in Figure 4b. Over the latter half of the simulation period, the average latitude for the oscillating case is 52°N, significantly farther south than its final position at the end of the simulation of 70°N, at which we compare its ozone to that of the tangential case. The associated ozone approaches a value just over 6 ppmv (seen in Figure 4a), consistent with the predicted photochemical equilibrium value for this latitude (see Figure 3). This behavior suggests that it is valid to consider the oscillating parcel as equivalent to one asymptotically approaching 52°N in order to determine its associated equilibrium ozone value. The associated running average production and loss are plotted as the dark gray lines in Figure 4c. These averages can be directly compared with the production and loss of the tangential case (Figure 4d). The difference between loss and production for the oscillating case is significantly less, on average, than for the tangential case and explains the resulting ozone difference. By the end of the 24–day period, the average production and loss for the oscillating parcel (the dotted lines in Figure 4) are approximately equal, suggesting that ozone has achieved an effective equilibrium value. The ozone in such parcels therefore exceeds that of their tangential counterparts, despite the fact that they can be found at the same latitude.

This study demonstrates that meridional ozone gradients may exist due solely to the differing dynamical histories of neighboring air parcels, as was also shown by *Tuck* [1979] and *Pyle and Rodgers* [1980]. The difference in behavior of the oscillating and tangential parcels in the conceptual model study is similar to that of parcels outside and inside the anticyclone and is central to the appearance of the low-ozone pockets.

5. Further Discussion

5.1. Vertical Extent

To understand the vertical boundaries of the low-ozone pockets (20–2 mbar), we examine the photochemical lifetime of ozone as a function of latitude and potential temperature (shown in Figure 1), as determined from the Goddard three-dimensional (3D) chemistry and transport model [*Douglass et al.*, 1996]. Below 20 mbar (~750 K), the ozone photochemical lifetime is long (approximately months) in the winter hemisphere unless aerosols (most notably polar stratospheric clouds) are present. With the exception of the winter polar vortex regions, therefore, ozone tends to be dynamically controlled and is conserved along the air parcel trajectories. Above 2 mbar (~1250 K), the ozone lifetime is short (approximately a day or less). Rapid photochemistry maintains an ozone mixing ratio near photochemical equilibrium at these higher altitudes regardless of transport. The layer in which these ozone pockets evolve is one in which the photochemical lifetime of ozone is similar in magnitude to the duration of strong containment provided by dynamical features such as the Aleutian anticyclone. The near balance between these photochemical and dynamical timescales makes the development of the low-ozone pockets possible at these altitudes.

5.2. Nitric Acid

Another characteristic of these low ozone pockets are the associated high values of HNO_3 reported by *Manney et al.* [1995] and *Rood et al.* [1993]. CLAES observes and the model predicts low values of HNO_3 in the tropics and along the boundary of the polar vortex (not shown). In the region surrounding the pocket of low ozone, both CLAES and the model indicate a significant enhancement of HNO_3, although the CLAES observations suggest ~30% more nitric acid within the pocket than the model. We are currently investigating the cause of this discrepancy. Model HNO_3/NO_y values in the tropics and midlatitudes are consistent with UARS data reported by *Morris et al.* [1997]. In the anticyclone, model HNO_3/NO_y appears to be ~10% higher than that of the surrounding air masses.

5.3. Sensitivity Studies

Our initialization scheme, though approximate, produces reliable results because the model is not particularly sensitive to small changes in the chemical initialization. Below we discuss the impact of changes in initial ozone, overhead ozone, temperature, NO_y, and Cl_y on the model results. Estimates of the accuracy uncertainties associated with each of the individual UARS measurements can be found in Table 1. Precision uncertainties from our initialization are comparatively small due to the large number of data points included in the zonal mean calculations.

Trajectory studies identify the tropics or subtropics as the main source for the air within the anticyclone. The same studies also suggest that some midlatitude air becomes entrained during the development of the anticyclone as well. Despite different origins and initial chemical compositions, however, all the parcels within the anticyclone end up with similarly low values of ozone by the end of the study period. Qualitatively, the trajectory analyses suggest that the specific origin of the air within the anticyclone is not the most important factor in determining the final value of ozone.

Quantitatively, we examine the effect of initial ozone on the final model ozone for 24–day calculations and find that the model shows a 5% response to a 10% change in ozone initial value. Given the estimated uncertainties in the MLS ozone data, the effect on our results is likely to be less than 5%.

We also tested the effect of changes in overhead column ozone. Again, using identical trajectories, ~ 18% increases in overhead column ozone result in ~4% decreases in the final model ozone values. Since parcels within the ozone pockets generally are found in columns with slightly less total ozone than those outside the pockets, such changes are counter to the observations. Changes in column ozone have little impact on the model calculations and oppose the changes associated with the low-ozone pockets.

Manney et al. [1995] also note that the ozone pockets appear downstream of the warm region. An examination of air parcel trajectories for the February–March 1993 event reveals that not only did parcels within the low ozone pocket pass through the warm region, but some parcels outside the pocket did also. These latter parcels did not experience the dramatic ozone losses associated with the anticyclone. While ozone and temperature are fundamentally interrelated through formation rate constants, the trajectory calculations suggest that the temperature differences are not responsible for the appearance of the low-ozone pockets.

To examine the impact of temperature on model ozone quantitatively, we ran 24–day, fixed temperature calculations. Our sensitivity analysis reveals 6% decreases in ozone associated with temperature increases from ~ 229 K to ~ 234 K. This temperature range roughly corresponds to the difference in the average temperatures along 7–day back trajectories for high-latitude air parcels outside and inside the pocket. Since the observed differences between ozone within the pocket and outside the pocket are of the order of 25%, differences in the temperature history of air parcels inside and outside the pockets cannot be the most important factor in their observed ozone differences.

Finally, we examine the impact of varying NO_y and Cl_y by ±30%, an amount consistent the uncertainty in the UARS data (see Table 1) and with the observed global variability of these quantities near 30 km [*Morris et al.*, 1997]. Our study suggests that although model ozone responds approximately linearly to changes in NO_y and Cl_y over this range, the sensitivity of the model to these changes is quite small: $(\Delta O_3/O_3)/(\Delta Cl_y/Cl_y)$ is ~–0.13 and $(\Delta O_3/O_3)/(\Delta NO_y/NO_y)$ is ~–0.34. If we are 20% uncertain about our initialization of both NO_y and Cl_y, the total resultant uncertainty in our model predictions for ozone remains less than 10%, an amount much smaller than the observed ozone change.

5.4. Other Cases

We have examined two other cases in some detail: September 1992 in the southern hemisphere and December 1992 in the northern hemisphere. The latter of these two cases was also described by *Manney et al.* [1995]. Figures 5 and 6 show comparisons of the zonal mean results from MLS and the model for these two cases, respectively.

For the September 1992 case, the low-ozone region appears near 45°S latitude and 180°–210°E longitude with values of ozone about 15% below the zonal mean. For the December 1992 case, the low ozone pocket appears near 40°N latitude and 180°–210°E longitude with ozone values similar to those observed in the vortex during this time period (4–5 ppmv). As noted by *Manney et al.* [1995], ozone gradients between the low-ozone pockets and the surrounding air masses are not as large in the southern hemisphere as those observed in the northern hemisphere.

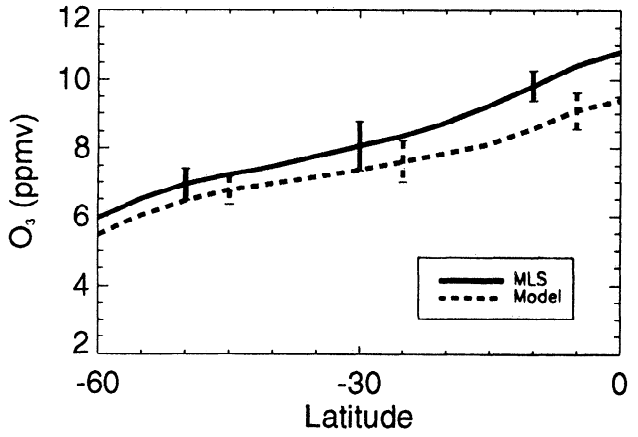

Figure 5. Zonal mean model and MLS ozone as a function of latitude in the southern hemisphere on the 850 K surface at 1200 GMT on September 8, 1992 (as in Figure 3). Polar values are not shown.

Figures 5 and 6 indicate that the model reliably reproduces the observed ozone gradients in both cases, although the model ozone values are systematically lower than the MLS observations in the southern hemisphere and considerably lower than MLS in the tropics. As in the March 1993 case, the model reproduces MLS observations of pockets relatively low in ozone compared with the zonal mean for both cases. The magnitude of ozone in the pockets in these cases, however, appears 10–20% higher than the MLS observations. Nevertheless, the explanation for their formation and appearance is consistent with the results of the February–March 1993 case.

6. Conclusions

Low-ozone pockets form subsequent to stratospheric warming events and consist not of air from the vortex (where ozone is already low), but rather, mainly of air

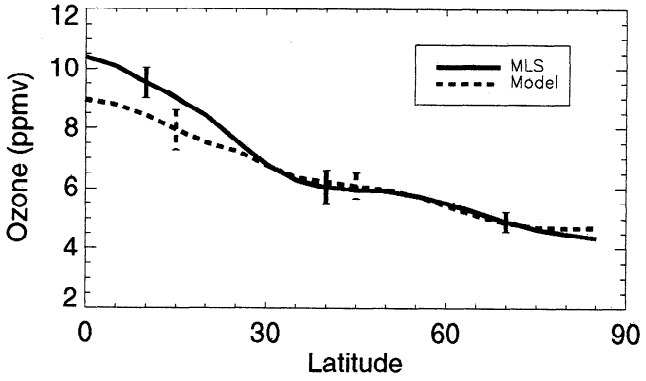

Figure 6. Zonal mean model and MLS ozone as a function of latitude in the northern hemisphere on the 850 K surface at 1200 GMT on December 29, 1992 (as in Figure 3).

from higher altitudes and lower latitudes (near the tropics and subtropics where ozone mixing ratios are high). These conclusions have been demonstrated by our trajectory analysis, the MLS water vapor data, and the study of *Manney et al.* [1995].

The pockets exist in a confined vertical layer of the stratosphere in which the ozone lifetime is comparable to the period of the confinement of air masses within a strong anticyclone. Using a Lagrangian chemical model and an initialization based upon UARS data, we have demonstrated that the primary mechanism behind the development of the low-ozone pockets is dynamical isolation of air at high latitudes for periods of time long enough that the local photochemical equilibrium can be approached. Surrounding air parcels are free to move north and south and therefore maintain ozone concentrations more consistent with lower-latitude equilibrium values. Differences in the dynamical histories of these two types of air parcels are indicated by the relative solar exposures calculated along back trajectories. Parcels in the low-ozone pockets experienced limited solar exposure, suggesting their confinement to high latitudes for an extended period of time. Surrounding air parcels experienced more solar exposure, suggesting a significant presence at lower latitudes during the study period.

Model sensitivity studies reveal that the temperature history and the specific chemical initialization (including O_3, overhead column O_3, NO_y, and Cl_y) are less important in development of the low-ozone pockets than is the isolation at high latitudes. By correctly predicting the magnitude of the observed ozone loss, the model simulation demonstrates that the ozone pockets are consistent with our current understanding of chemistry and dynamics and successfully addresses the issues raised by *Manney et al.* [1995].

Acknowledgments. G.A.M. acknowledges support from National Research Council–NASA Goddard Space Flight Center Research Associateship Program. Funding has also been provided by the UARS Guest Investigator Program. Thanks to Jim Russell and the HALOE team for use of the HALOE data, to Aiden Roche and the CLAES team for use of the CLAES data, to Paul Newman and Leslie Lait for the NCEP wind fields used in the trajectory calculations, and to David Considine, Eugene Cordero, Andy Dessler, Charlie Jackman, Rich Stolarski, and two anonymous reviewers for helpful comments.

References

Anderson, D.E., R. Demajistre, S.A. Lloyd, and P.K. Swaminathan, Impact of aerosols and clouds on the troposphere and stratosphere radiation field with application to twilight photochemistry at 20 km, *J. Geophys. Res., 100*, 7135–7145, 1995.

Brasseur, G., and S. Solomon, *Aeronomy of the Middle Atmosphere*, D. Reidel, Norwell, Mass., 1984.

Cunnold, D.M., H. Wang, W.P. Chu, and L. Froidevaux, Comparisons between Stratospheric Aerosol and Gas Experiment II and Microwave Limb Sounder ozone measurements and aliasing of SAGE II ozone trends in the lower stratosphere, *J. Geophys. Res., 101*, 10,061–10,075, 1996.

DeMore, W.B., et al., Chemical kinetics and photochemical data for use in stratospheric modeling, *JPL Publ., 94-26*, 1994.

Dessler, A.E., et al., Correlated observations of HCl and $ClONO_2$ from UARS and implications for stratospheric chlorine partitioning, *Geophys. Res. Lett., 22*, 1721–1724, 1995.

Douglass, A.R., C.J. Weaver, R.B. Rood, and L. Coy, A three dimensional simulation of the ozone annual cycle using winds from a data assimilation system, *J. Geophys. Res., 101*, 1463–1474, 1996.

Douglass, A.R., R. Rood, S.R. Kawa, and D.J. Allen, A 3D simulation of the evolution of the middle latitude winter ozone in the middle stratosphere, *J. Geophys. Res., 102*, 19,217–19,232, 1997.

Froidevaux, L., et al., Validation of UARS Microwave Limb Sounder ozone measurements, *J. Geophys. Res., 101*, 10,017–10,060, 1996.

Gordley, L.L., et al., Validation of nitric oxide and nitrogen dioxide measurements made by the Halogen Occultation Experiment for UARS platform, *J. Geophys. Res., 101*, 10,241–10,266, 1996.

Holton, J.R., An Introduction to Dynamic Meteorology, San Diego: Academic Press, 1992.

Kawa, S. R., et al. Interpretation of NO_x/NO_y observations from AASE II using a model of chemistry along trajectories, *Geophys. Res. Lett., 20*, 2507–2510, 1993.

Kumer, J.B., et al., Comparison of correlative data with HNO_3 version 7 from the CLAES instrument deployed on the NASA Upper Atmosphere Research Satellite, *J. Geophys. Res., 101*, 9621–9656, 1996.

Lahoz, W.A., et al., Validation of UARS Microwave Limb Sounder 183-GHz H_2O measurements, *J. Geophys. Res., 101*, 10,129–10,149, 1996.

Leovy, C. B., et al., Transport of ozone in the middle stratosphere: Evidence for planetary wave breaking, *J. Atmos. Sci., 42*, 230–244, 1985.

LeTexier, H., S. Solomon, and R.R. Garcia, The role of molecular hydrogen and methane oxidation in the water vapour budget of the stratosphere, *Q. J. R. Meteorol. Soc., 114*, 281–295, 1988.

Manney, G.L., L. Froidevaux, J.W. Waters, R.W. Zurek, J.C. Gille, J.B. Kumer, J.L. Mergenthaler, A.E. Roche, A. O'Neill, and R. Swinbank, Formation of low ozone pockets in the middle stratosphere anticyclone during winter, *J. Geophys. Res., 100*, 13,939–13,950, 1995.

Mergenthaler, J.L., et al., Validation of CLAES $ClONO_2$ measurements, *J. Geophys. Res., 101*, 9603– 9620, 1996.

Morris, G.A., et al., Trajectory mapping and applications to data from the Upper Atmosphere Research Satellite, *J. Geophys. Res., 100*, 16,491–16,505, 1995.

Morris, G.A., D.B. Considine, A.E. Dessler, S.R. Kawa, J. Kumer, J. Mergenthaler, A. Roche, and J.M. Russell, III, Nitrogen partitioning in the middle stratosphere as observed by the Upper Atmosphere Research Satellite, *J. Geophys. Res., 102*, 8955–8965, 1997.

Newman, P. A., et al., Meteorological atlas of the southern hemisphere lower stratosphere for August and September 1987, *NASA Tech. Memo. 4049*, 1988.

Pyle, J.A., and C.F. Rodgers, Stratospheric transport by stationary planetary waves–The importance of chemical processes, *Q. J. R. Meteorol. Soc., 106*, 421–446, 1980.

Randel, W. J., The evolution of winds from geopotential height data in the stratosphere, *J. Atmos. Sci., 44*, 3097–3120, 1987.

Roche, A.E., et al., Validation of CH_4 and N_2O measurements by the cryogenic limb array etalon spectrometer instrument on the Upper Atmosphere Research Satellite, *J. Geophys. Res., 101*, 9679–9710, 1996.

Rood, R.B., A.R. Douglass, J.A. Kaye, and D. B. Considine, Characteristics of wintertime and autumn nitric acid chemistry as defined by Limb Infrared Monitor of the Stratosphere (LIMS) data, *J. Geophys. Res., 98*, 18,533–18,545, 1993.

Rosenfield, J. E., A simple parameterization of ozone infrared absorption for atmospheric heating rate calculations, *J. Geophys. Res., 96*, 9065–9074, 1991.

Russell, J. M., III, et al., Validation of hydrogen chloride measurements made by the Halogen Occultation Experiment from the UARS platform, *J. Geophys. Res., 101*, 10,151–10,162, 1996.

Schoeberl, M. R., and L. C. Sparling, Trajectory modeling, in *Diagnostic Tools in Atmospheric Physics, Proceedings of the International School of Physics, Enrico Fermi, Course CXVI*, edited by G. Fiocco and G. Visconti, pp. 289–305, North–Holland, New York, 1995.

Shine, K.P., The middle atmosphere in the absence of dynamic heat fluxes, *Q. J. R. Meteorol. Soc., 113*, 603–633, 1987.

Stolarski, R.S., et al., 1995 scientific assessment of the atmospheric effects of stratospheric aircraft, *NASA Ref. Publ. 1381*, 1995.

Tuck, A.F., A comparison of one-, two- and three-dimensional model representations of stratospheric gases, *Philos. Trans. R. Soc. London A., 290*, 477–494, 1979.

A.R. Douglass, S.R. Kawa, and M.R. Schoeberl, Code 916, NASA Goddard Space Flight Center, Greenbelt, MD 20771.

L. Froidevaux and J. Waters, Jet Propulsion Laboratory, California Institute of Technology, 4800 Oak Grove Drive, Pasadena, CA 91109.

G.A. Morris, Joint Center for Earth Systems Technology, University of Maryland Baltimore County, Baltimore, MD 21250. (e-mail: morris@zephyr.gsfc.nasa.gov)

(Received November 13, 1996; revised September 2, 1997; accepted September 3, 1997.)